Supplementary section

To show that our way of sampling is robust, we have compared the most recent version of spatially downscaled GOME-2 SIF (GSIF; 8 day GOME-2 downscaled SIF of 0.05*0.05 resolution at 740nm; [1]) means with the OCO-2 SIF means. The percentage change in 2018 from both downscaled GOME-2 SIF (GSIF) and OCO-2 was comparable (Table A1). This shows that although OCO-2 does not have a fixed revisit time, and has different measurement modes (nadir and glint). Aggregated mean values (of all the different measurement modes) over a continental scale are robust for multi-year comparison.

Table S1. Comparison of anomalies (2018 – Mean*) in GSIF [1] and OCO-2 SIF measurement (used in this study) for three different areas.

	Anomaly (in %)	
Aggregated Area	**GSIF**	**OCO-2 measurements**
Heatwave	-28.91	-31.04
Spring-Drought Area	6.20	4.90
Summer-Drought Area	-10.98	-12.65

* Mean refers to year 2015-2017

Table S2: Percentage of Nadir OCO-2 measurements mode for the Mean years (2015-2017) and 2018, from total OCO-2 measurements (Nadir + Glint) mode used in the study.

	% Nadir mode	
Land-cover	**Mean (2015-2017)**	**2018**
Agricultural	50.8	51.2
Broadleaf Forest	50.3	50.1
Coniferous Forest	51.1	51.5
Mixed Forest	52.1	52.7

Table S3: Relative vegetation class area in percentage for drought and non-drought area

Vegetation type (%)	**Drought Area**	**Non-Drought Area**
Agricultural area	53.2	57.4
Broadleaved Forest	4.2	21.4
Coniferous	37.4	16.4
Mixed Forest	5.2	4.8

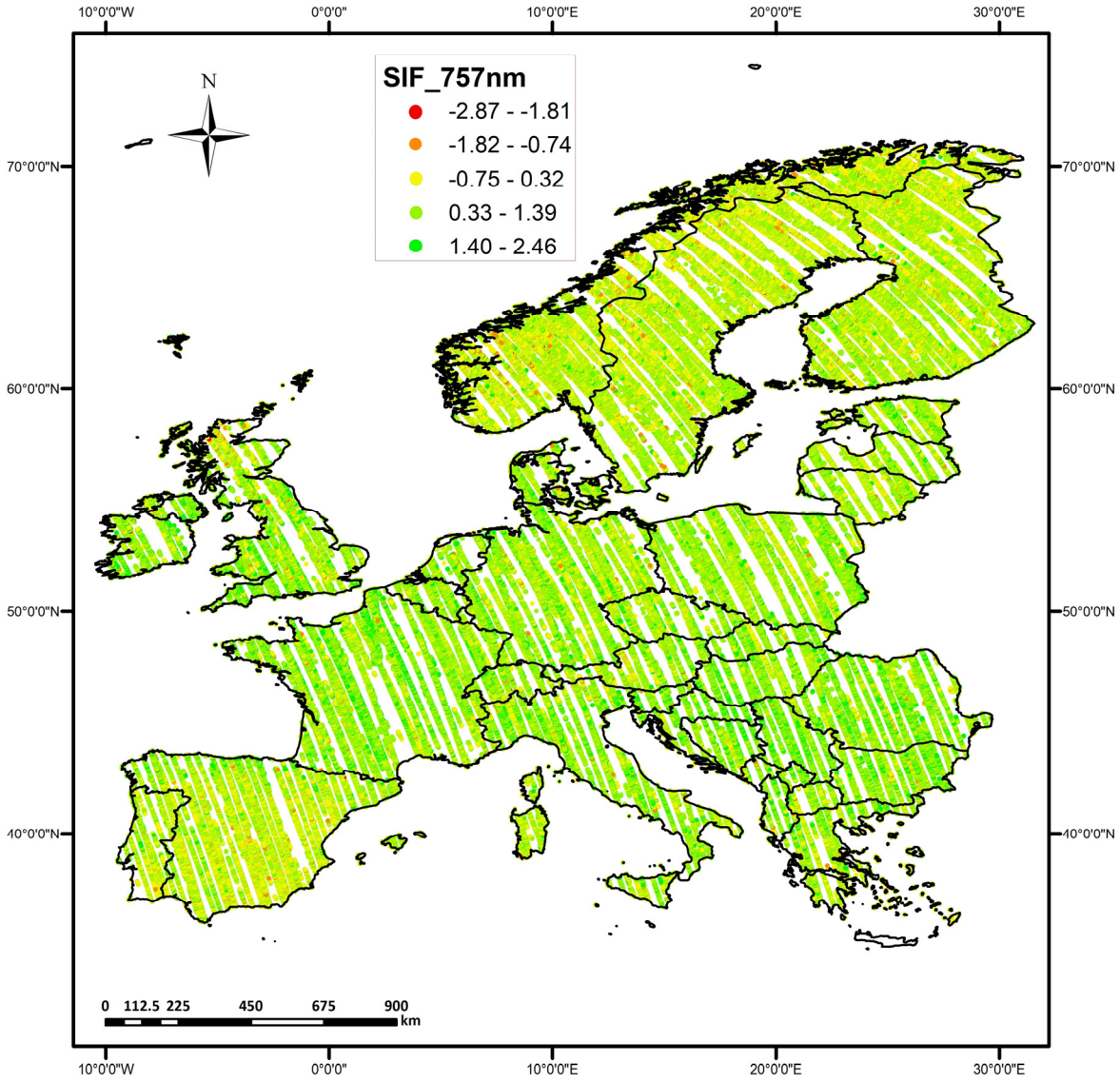

Figure S1. Illustration of the spatial distribution and orbit track of OCO-2 SIF soundings of spring and summer season for Europe in 2018. The temporal resolution is 16 days. The SIF values are retrieved at 757 nm (SIF_{757}; units - $W/m^2/sr/\mu m$)

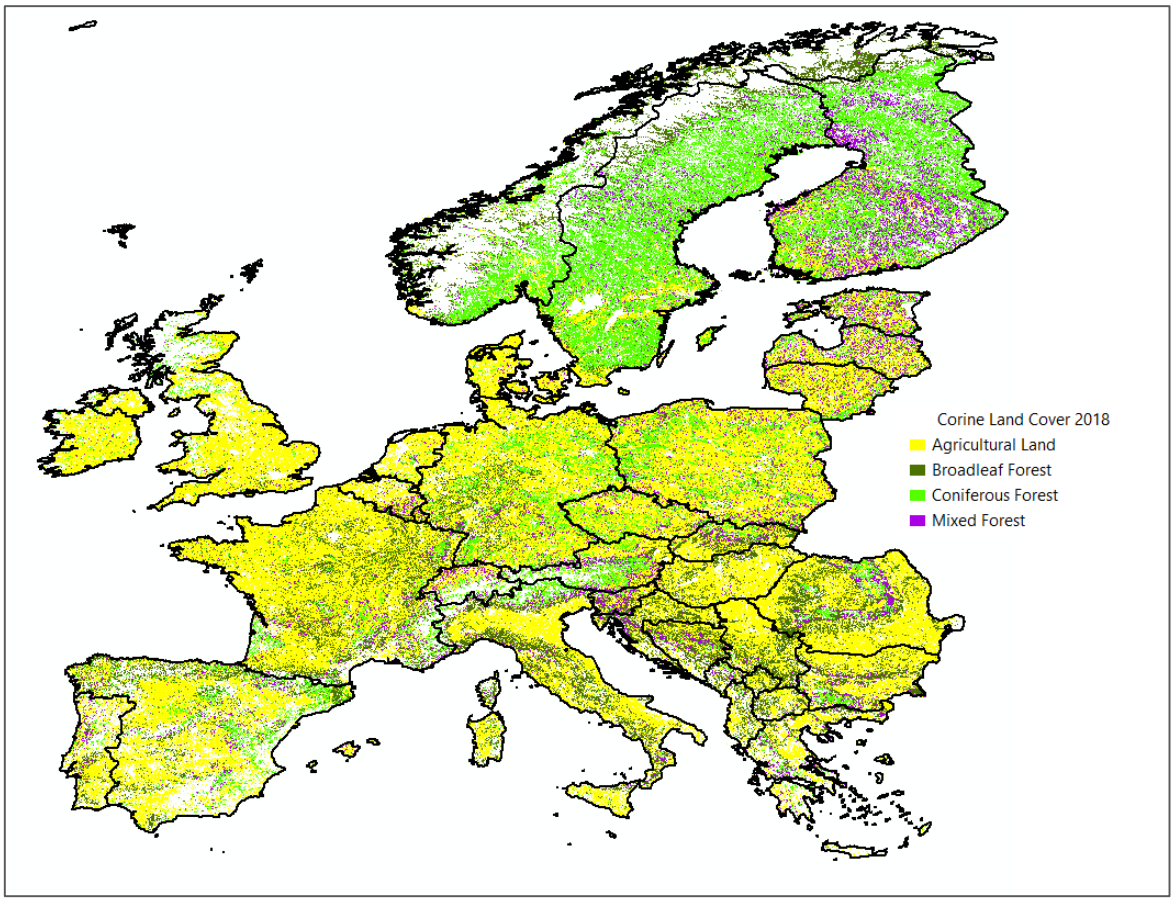

Figure S2. Land cover map of Europe showing agriculture, broadleaf forest, coniferous forest and mixed forest based on Corine Land Cover (CLC) 2018, version 20b2.

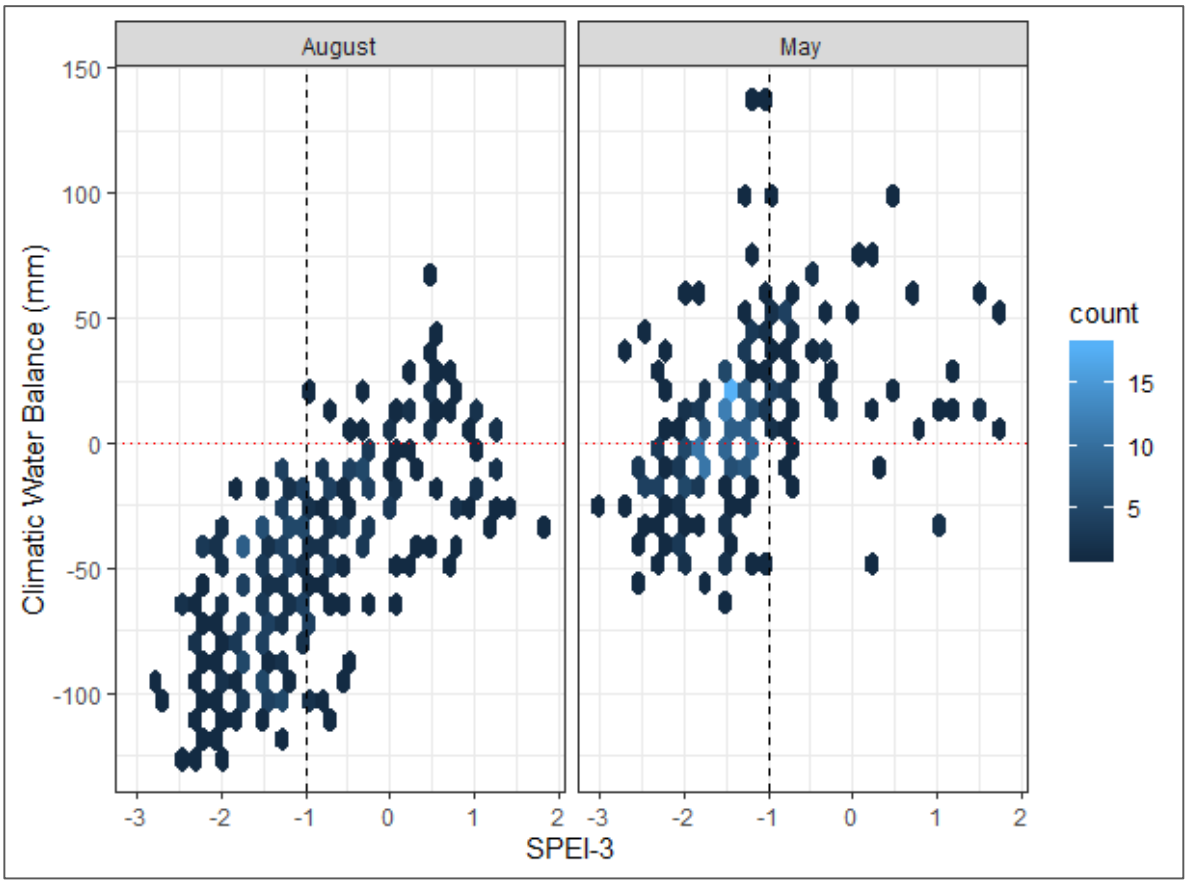

Figure S3: Representation of climatic water balance (CWB) by the SPEI-3 values during spring (May month) and summer (August month). The vertical line represents the SPEI-3 threshold for defining drought conditions in the study area.

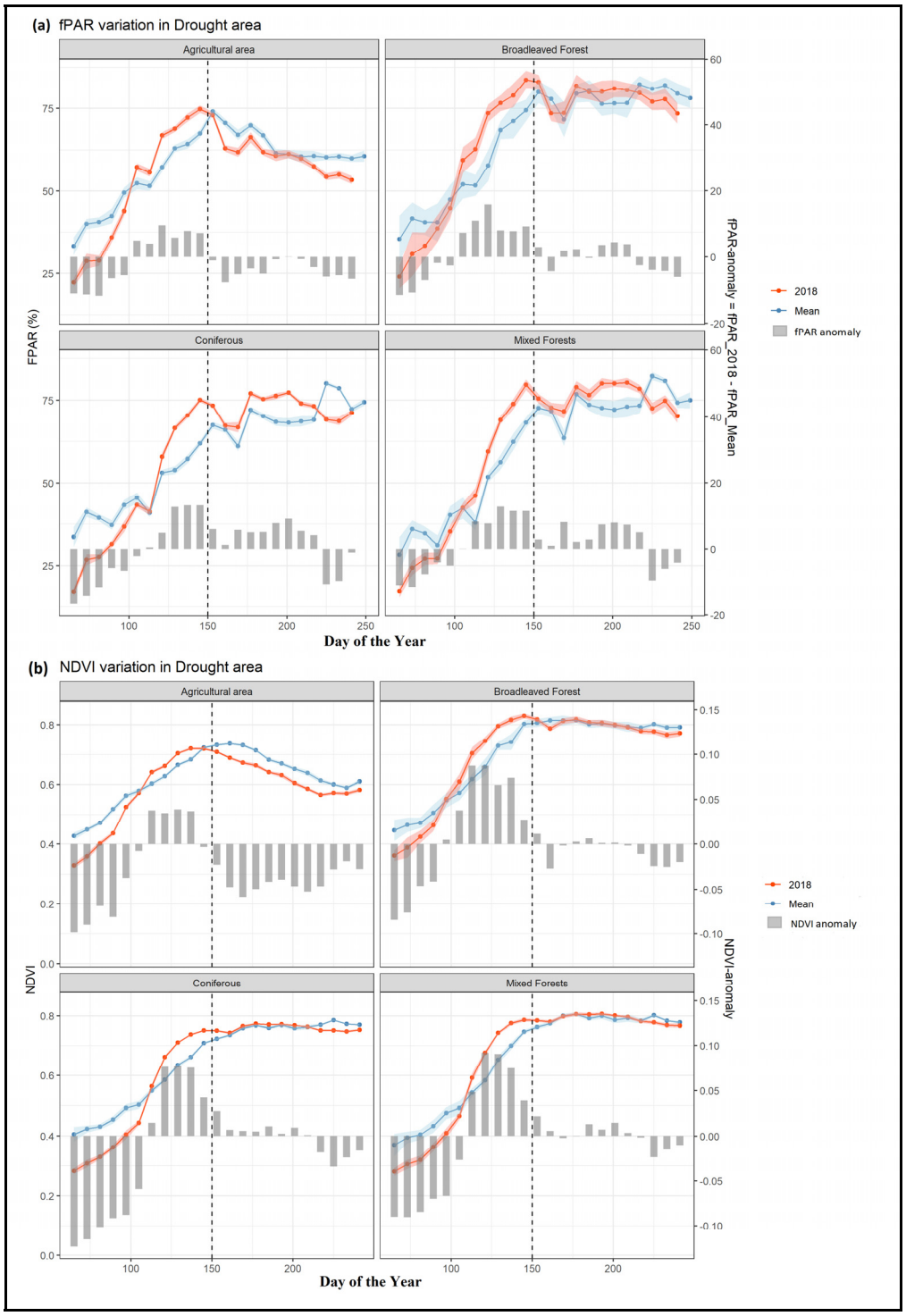

Figure S4. Variation of (a) fPAR and (b) NDVI for drought area across different vegetation types as observed from MODIS fPAR product (MYD15A2H) version 6 and MODIS NDVI product (MOD/MYD13Q1) version 6. The fPAR and NDVI values are sampled from the OCO-2 SIF footprint and are spatially and temporally averaged for three previous years (2015-2017; 'Mean') and year 2018 ('2018'). fPAR anomalies (fPAR_2018 – fPAR_Mean) and NDVI anomalies (NDVI_2018 – NDVI_Mean) are represented by gray bars. The left and right side of vertical solid line represents spring and summer season, respectively.

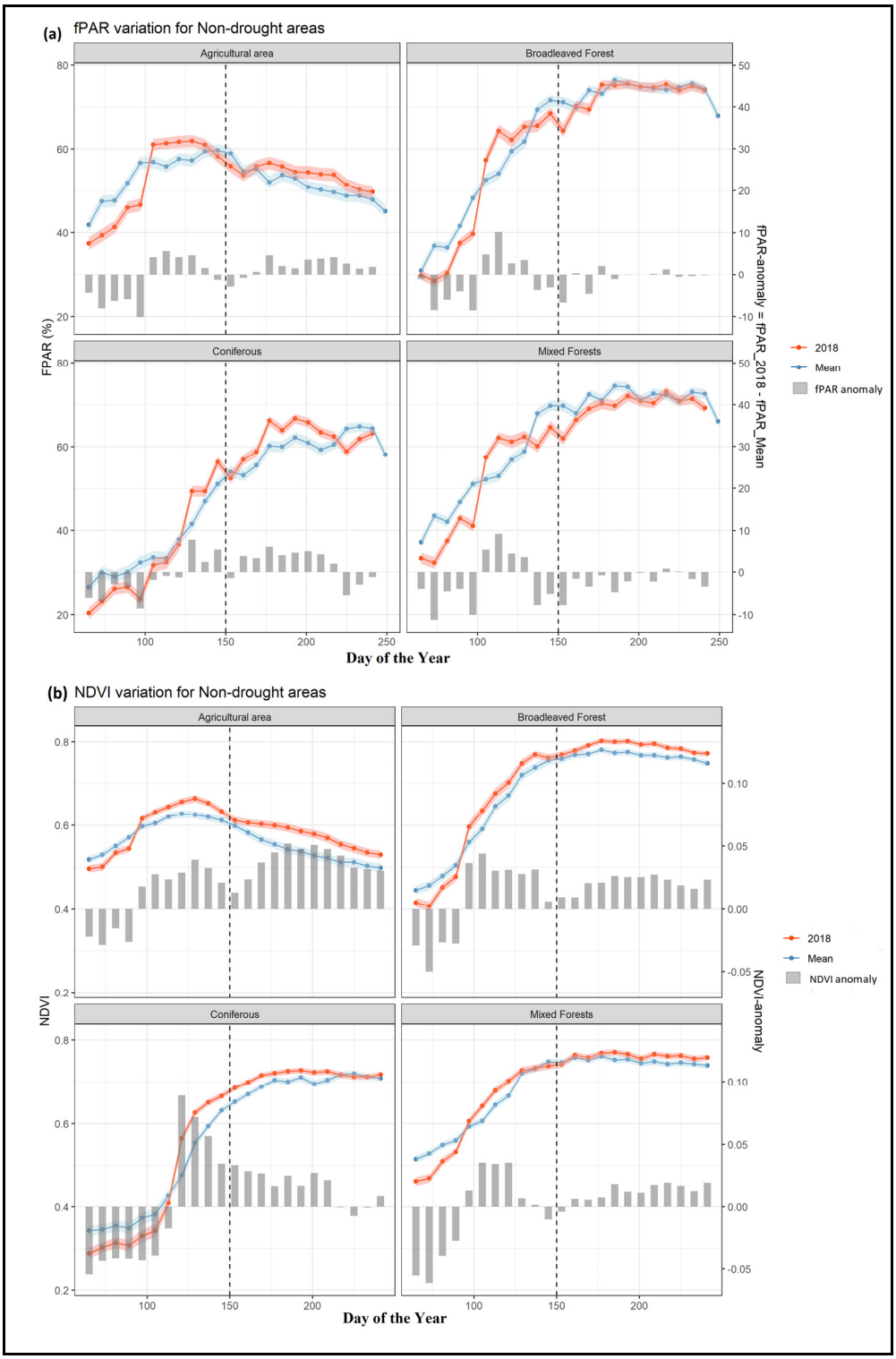

Figure S5: Variation of (a) fPAR and (b) NDVI for non-drought area across different vegetation types as observed from MODIS fPAR product (MYD15A2H) version 6 and MODIS NDVI product (MOD/MYD13Q1) version 6. The fPAR and NDVI values are sampled from the OCO-2 SIF footprint and are spatially and temporally averaged for three previous years (2015-2017; 'Mean') and year 2018 ('2018'). fPAR anomalies (fPAR_2018 – fPAR_Mean) and NDVI anomalies (NDVI_2018 – NDVI_Mean) are represented by gray bars. The left and right side of vertical solid line represents spring and summer season, respectively.

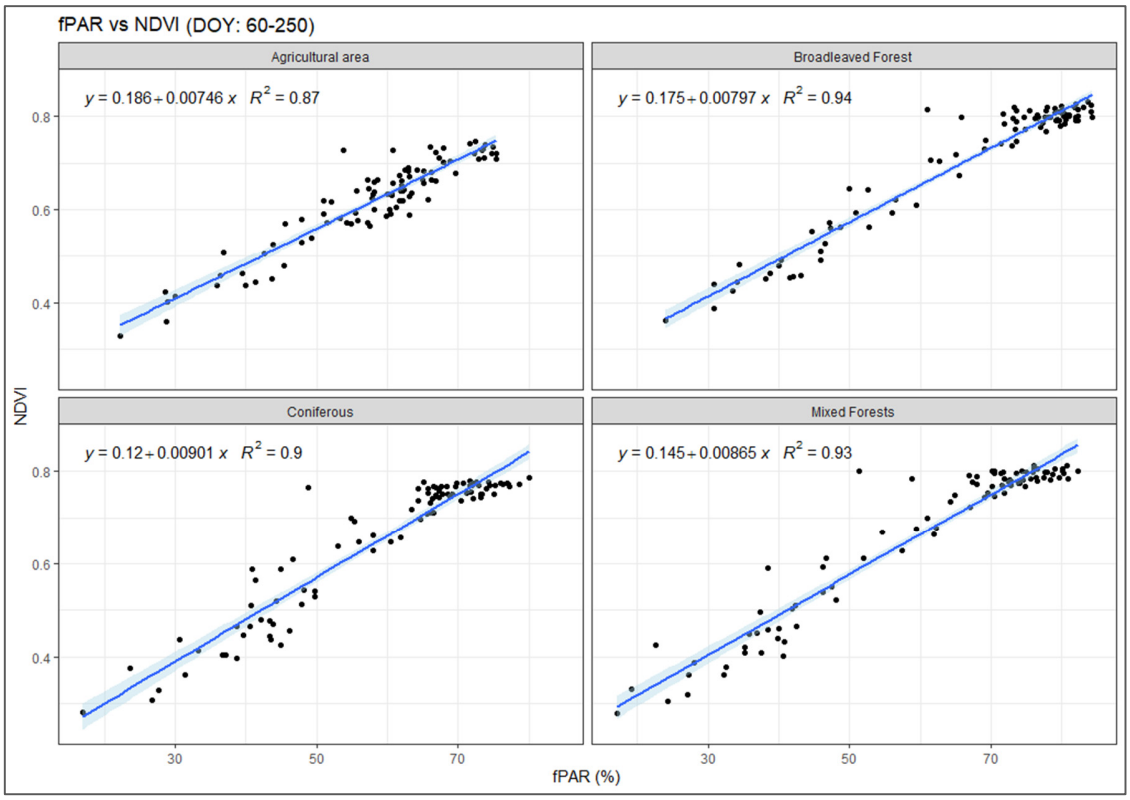

Figure S6. Relationship between fPAR and NDVI for different vegetation types.

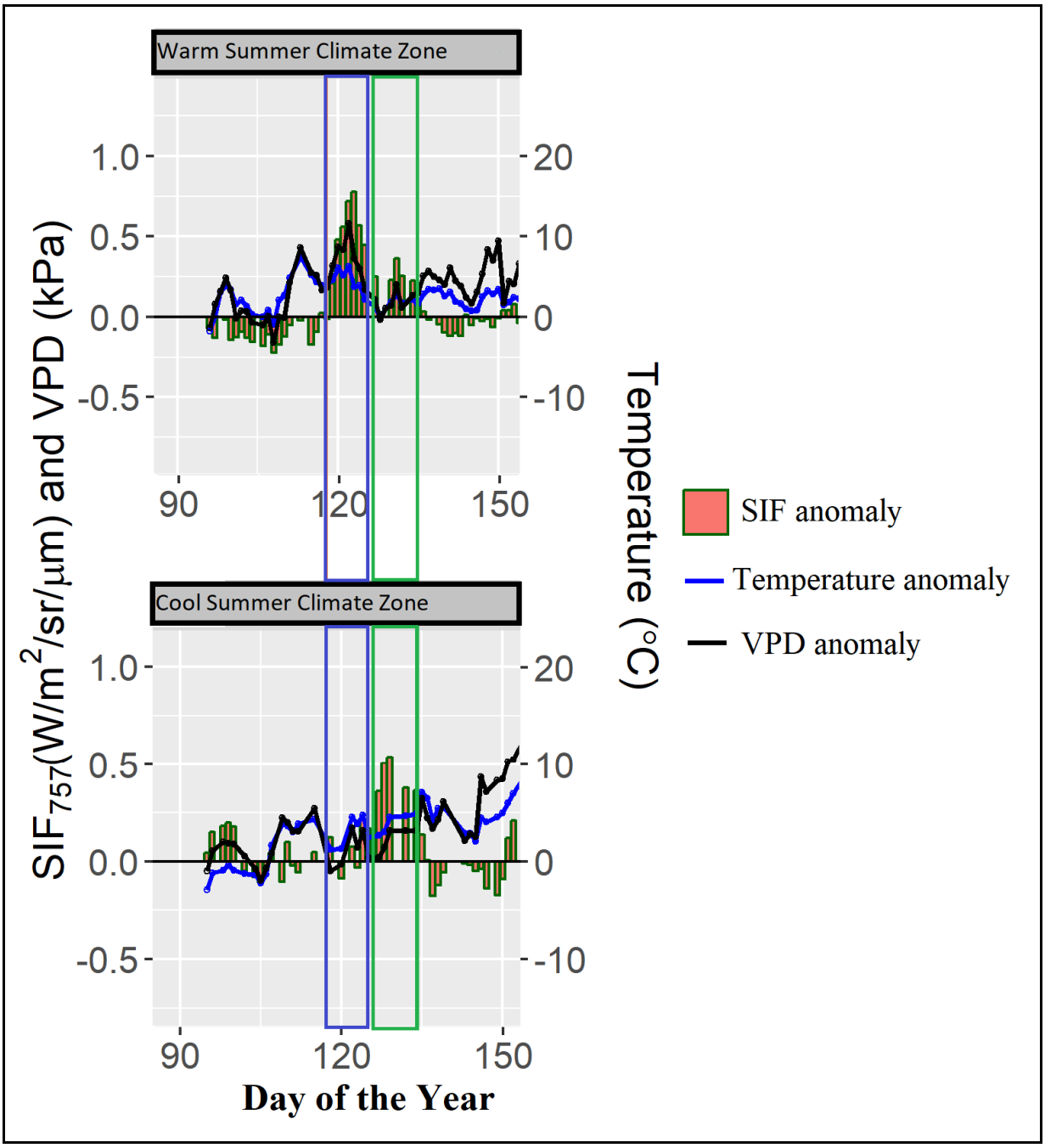

Figure S7. Two peaks in the broadleaved forest during summer resulting from a different timing in leaf flushing in the warm summer (Central Europe, blue box) and cool summer (Northern Europe, green box) climate zones of the drought area. Climate zones are based on Köppen-Geiger climate classification [2]

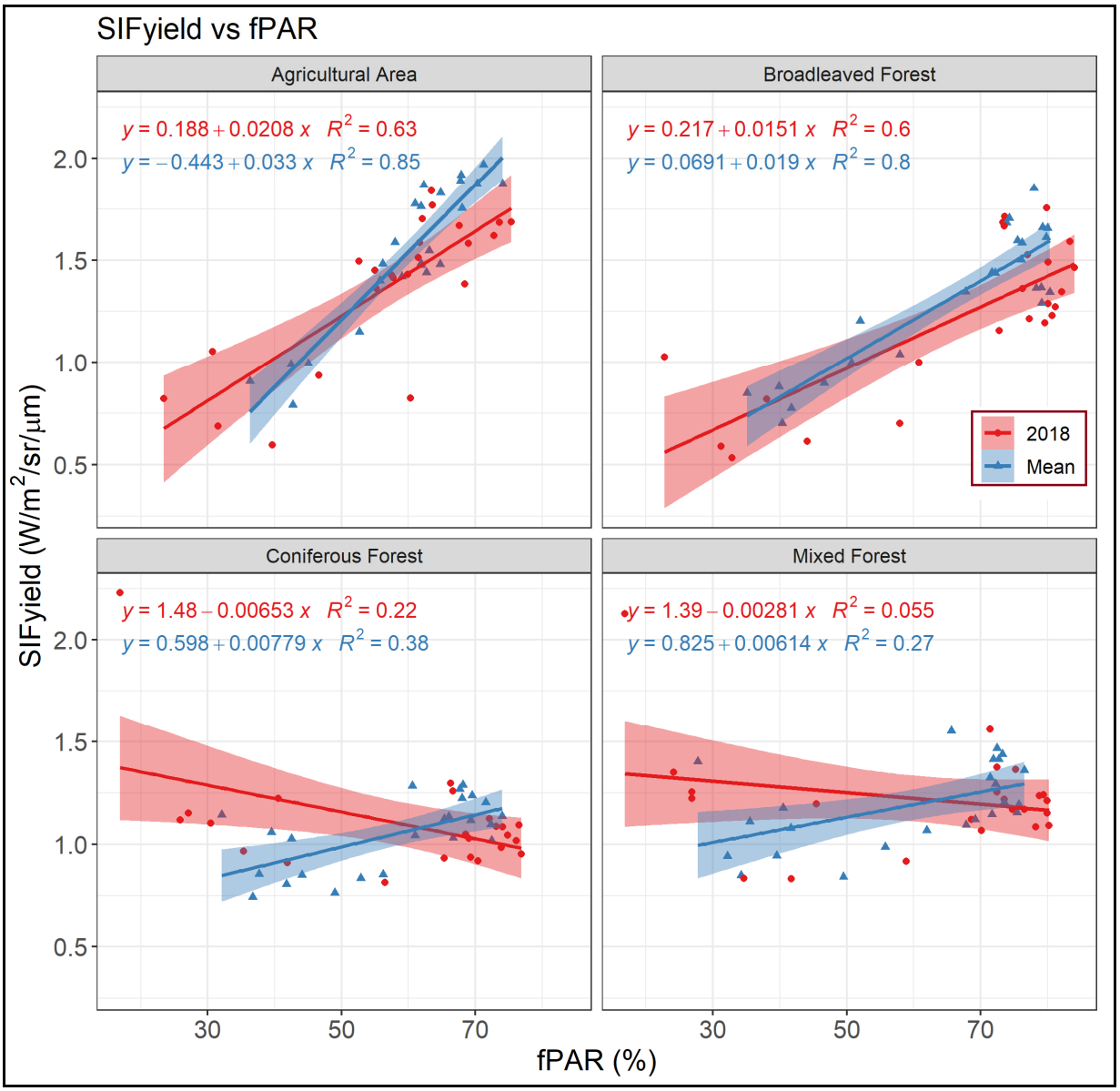

Figure S8. Relationship between SIF_{yield} and fPAR across different vegetation types. The fPAR values are sampled from the OCO-2 SIF footprint and are spatially and temporally averaged for three previous years (2015-2017; 'Mean') and year 2018 ('2018'). SIFyield is calculated based on equation 1.

References

1. Duveiller, G.; Filipponi, F.; Walther, S.; Köhler, P.; Frankenberg, C.; Guanter, L.; Cescatti, A. A spatially downscaled sun-induced fluorescence global product for enhanced monitoring of vegetation productivity. *Earth Syst. Sci. Data* **2020**, doi:10.5194/essd-12-1101-2020.

2. Rubel, F.; Brugger, K.; Haslinger, K.; Auer, I. The climate of the European Alps: Shift of very high resolution Köppen-Geiger climate zones 1800-2100. *Meteorol. Zeitschrift* **2017**, doi:10.1127/metz/2016/0816.